

<https://doi.org/10.1038/s41612-024-00668-4>

Decomposition of physical processes controlling EASM precipitation changes during the mid-Piacenzian: new insights into data–model integration

Check for updates

Yong Sun^{1,2}✉, Haibin Wu^{3,4}, Lin Ding¹, Lixin Chen³, Christian Stepanek⁵, Yan Zhao¹, Ning Tan³, Baohuang Su⁶, Xiayu Yuan⁷, Wenchao Zhang⁸, Bo Liu⁹, Stephen Hunter¹⁰, Alan Haywood¹⁰, Ayako Abe-Ouchi¹¹, Bette Otto-Bliesner¹², Camille Contoux², Daniel J. Lunt¹³, Aisling Dolan¹⁰, Deepak Chandan¹⁴, Gerrit Lohmann^{5,15}, Harry Dowsett¹⁶, Julia Tindall¹⁰, Michiel Baatsen¹⁷, W. Richard Peltier¹⁴, Qiang Li¹⁸, Ran Feng¹⁹, Ulrich Salzmann²⁰, Wing-Le Chan¹¹, Zhongshi Zhang^{9,21}, Charles J. R. Williams¹³ & Gilles Ramstein²

The mid-Piacenzian warm period (MPWP, ~3.264–3.025 Ma) has gained widespread interest due to its partial analogy with future climate. However, quantitative data–model comparison of East Asian Summer Monsoon (EASM) precipitation during the MPWP is relatively rare, especially due to problems in decoding the imprint of physical processes to climate signals in the records. In this study, pollen-based precipitation records are reconstructed and compared to the multi-model ensemble mean of the Pliocene Model Intercomparison Project Phase 2 (PlioMIP2). We find spatially consistent precipitation increase in most simulations but a spatially divergent change in MPWP records. We reconcile proxy data and simulation by decomposing physical processes that control precipitation. Our results 1) reveal thermodynamic control of an overall enhancement of EASM precipitation and 2) highlight a distinct control of thermodynamic and dynamical processes on increases of tropical and subtropical EASM precipitation, reflecting the two pathways of water vapor supply that enhance EASM precipitation, respectively.

It is well established that past climate change provides a reference for our future climate^{1–3}. Recent study has highlighted that a climate similar to that of the Pliocene will appear in near-term climate projections⁴. As a result, the climate of the Pliocene has received increasing attention in the paleoclimate community. Over the past 15 years, two phases of the Pliocene Model Intercomparison Project (PlioMIP) have been executed. This effort has been made possible by decades of research establishing environmental and geographical conditions of the Pliocene, in particular by means of the Pliocene Research, Interpretation and Synoptic Mapping (PRISM) initiative and has involved continued efforts in quantifying and understanding Pliocene climate from geological reconstructions and modeling^{5–14}. From PlioMIP we have gained a better understanding of the large-scale features and driving mechanisms of the mid-Piacenzian warm period (MPWP) that may be useful in the context of future climate

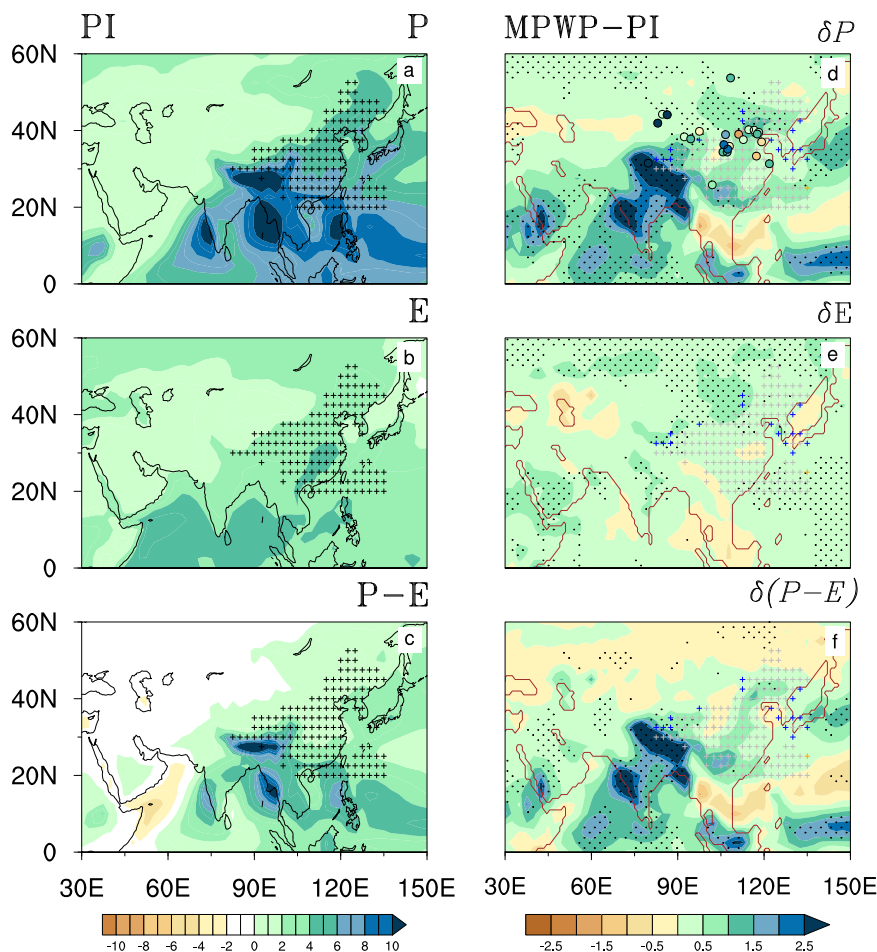
change. On the other hand the effort has provided opportunities for the cross-validation of regional climate patterns in records and simulations of this time period.

The East Asian summer monsoon (EASM) is a hybrid tropical and subtropical monsoon with characteristics different from a typical tropical monsoon^{15–18}. Monsoon circulation and precipitation are the two main aspects that characterize monsoon climate^{19,20}, and these are in the focus of studies of monsoon changes in the future by means of climate projections. Simulated future changes in the EASM show behavior that differs from that of other monsoon members²¹.

Despite the fact that precipitation is projected to increase in both EASM and other monsoon systems, the expected future strengthening of the EASM circulation is in contrast to projected weakening of the circulation in other monsoon regions^{22–25}. The combined effect of two climate characteristics must be considered in future EASM precipitation. Relative

A full list of affiliations appears at the end of the paper. ✉e-mail: yongsun@itpcas.ac.cn

Fig. 1 | Data and model comparison of EASM precipitation during the MPWP. Left panel: pre-industrial (PI) mean June–July–August (JJA) of three variables (from top to bottom: a precipitation (P), b evaporation (E), c precipitation minus evaporation (P–E)); units: mm/day) derived from the PlioMIP2 multi-model ensemble (MME); right panel: as left panel but for differences of three variables between mid-Piacenzian Warm Period (MPWP) and PI (d–f). Black dotted areas in the right panel indicate agreement of the MME with regard to precipitation anomaly, MPWP vs. PI (at least 10 out of 14 models show the same sign of precipitation change as the MME). Towards a quantitative data–model comparison the same color bar is used for recorded (colored circles; 25 pollen-based precipitation records, shown in the δP anomaly MPWP–PI) and simulated precipitation changes. According to the definition of ref. 21, the EASM domain is calculated separately for PI (black “+” symbol, left panel) and MPWP periods (colored “+” symbols, divided into three categories: common areas for both periods (gray “+”, right panel), expanding/shrinking areas during the MPWP relative to PI disentangled by different colors (blue/yellow “+”, right panel)). Black and yellow curves denote the coastlines of PI (left panel) and MPWP (right panel), respectively.



importance of increased water vapor transport, caused by enhanced circulation and surface warming, alternates with the temperature threshold²⁶. This means that the future EASM precipitation increase at lower temperature rise thresholds (i.e., for global warming targets of 1.5 °C and 2 °C above pre-industrial levels) is mainly under thermodynamic control, while dynamic processes related to strengthening of monsoon circulation play a more dominant role for temperature rise beyond 2 °C²⁶. In this study we would like to further explore this topic in the context of the Pliocene. Are thermodynamical or dynamical processes more relevant for EASM change in warmer equilibrium climates? Sun et al.²⁷ quantified the EASM dynamics under the ECP4.5 scenario with reference to the MPWP and yielded a thermodynamically controlled increase in future EASM precipitation²⁷. However, their conclusion is based on only one model from PlioMIP1 because PlioMIP1 lacks the complete set of variables required for moisture budget analysis. This limitation severely hampers the comparability of EASM dynamics between PlioMIP1 and PlioMIP2. Increased climate sensitivity has been documented for some models that contributed to PlioMIP2 but not to PlioMIP1^{13,27–29}. Consequently, particularly warm climate states may not be represented in the study by ref. 27. The PlioMIP2 ensemble offers the opportunity to re-examine EASM dynamics during the MPWP to improve our understanding of the mechanisms that may drive future EASM precipitation changes. With our study, we also overcome a shortcoming of previous PlioMIP1-based analyses of the EASM that are in lack of quantitative comparisons with reconstructions^{27,29–32}.

This study quantitatively compares changes in EASM precipitation during the MPWP as reconstructed from pollen records and as simulated by PlioMIP2 models and shows a clear data–model discrepancy. We present a new approach that can be used to reconcile data and models where we decompose the physical processes controlling monsoon precipitation changes and then spatially match proxy-recorded precipitation changes

with changes in the decomposed physical processes. Thereby we provide a physical interpretation of precipitation changes in the records. We highlight that thermodynamically controlled increase in water vapor transport leads to an overall enhancement of EASM precipitation, while thermodynamic and dynamical processes show contrasting dominant controls on tropical and subtropical EASM monsoon precipitation in the records and simulations during the MPWP.

Results

Quantitative data–model comparison: data–model disagreement

Towards conducting the data–model comparison, we first examine the mean state of the East Asian summer water vapor cycle for the PI period from the PlioMIP2 multi-model ensemble (MME). Following the definition by ref. 21, the MME PI EASM domain (black+, Fig. 1a–c) is in agreement with observations. We note that a net moisture flux convergence is required to maintain a humid climate in East Asia as precipitation exceeds evaporation in the area (shading, Fig. 1c).

The MME EASM domain during MPWP is almost unchanged compared to the PI period, apart from a weak expansion of the EASM margin. In contrast to negligible changes in EASM area, changes in the water cycle in the MPWP monsoon region relative to the PI period are evident (Fig. 1d–f). In agreement with elevated temperature in the atmosphere, precipitation and evaporation over East Asia are both simulated to increase in the MPWP compared to the PI period (Fig. 1d, e). As precipitation increases more than evaporation, we find intensified net rainfall, thus leading to a wetter MPWP East Asia (Fig. 1f) which is consistent with earlier studies using qualitative records that revealed a wetter East Asia condition during the MPWP^{27,29,30,32}.

Across the PlioMIP2 MME, there is a spatially consistent increase in EASM precipitation during the MPWP, while the precipitation response from individual model simulations is less in agreement with the MME,

especially in the EASM domain (Fig. 1d). Model uncertainty highlights the necessity of employing quantitative precipitation reconstruction as a model-independent source of information to validate reliability of simulated precipitation changes during the MPWP. However, pollen-based precipitation records and simulations are not well matched, as shown by inconsistent precipitation changes among records in contrast to a consistent precipitation increase derived from the climate simulations (Fig. 1d). The important question, that we would like to answer with this study, is how records, showing inconsistent precipitation changes, and models, suggesting a spatially consistent precipitation increase, may be reconciled. Our answer to this question is illustrated in the following section of this paper.

Decomposition of physical processes controlling EASM precipitation changes to reconcile data–model comparison

Using water vapor budget to reveal physical processes of EASM precipitation. Considering the spatial inhomogeneity of recorded precipitation and the multifaceted processes that affect precipitation, the decomposition of physical processes controlling monsoon precipitation is used to reconcile inferences from data and models. We analyze sources and sinks of water vapor in East Asia employing the moisture budget equation. In the mean moisture budget (Fig. 2a), evaporation and vertical moisture transport are the two main sources of water vapor in East Asia for both the PI and MPWP periods. The supply of water vapor to East Asia is largely balanced by precipitation (water vapor sinks), whereas the remaining terms (horizontal moisture transport and residual) contribute little to sources and sinks of water vapor in East Asia (Fig. 2a). As precipitation exceeds evaporation, this in turn leads to a humid East Asian monsoon climate for both periods (Fig. 2a).

Water vapor sources and sinks in East Asia differ between the two periods. Water vapor, which maintains the enhanced EASM precipitation, originates during MPWP mainly from enhanced vertical moisture transport, followed by the contribution of enhanced evaporation (Fig. 2b). However, signs of the horizontal moisture transport and of the residual term are uncertain across the PlioMIP2 models (Fig. 2b). Albeit both precipitation and evaporation in East Asia are elevated during the MPWP, the increase in precipitation outpaces that of evaporation, resulting in raised MPWP net precipitation in East Asia. We find that the vertical component of moisture transport dominates the horizontal component with regard to increased net precipitation during the MPWP (Fig. 2b). Most of the models (12 out of 14, except COSMOS and HadCM3), simulate an increase in EASM precipitation, which is consistent with the increase in precipitation in the MME (Fig. 2b). In contrast, COSMOS and HadCM3 simulate a decrease in EASM precipitation during the MPWP, mainly due to decrease in vertical moisture transport (Fig. 2b).

We separate changes in vertical and horizontal moisture transport into their respective thermodynamic (δTH ; changes in specific humidity at constant circulation; Fig. 2c) and dynamic (δDY ; changes in circulation at constant specific humidity; Fig. 2c) contributions and co-variations in both (not shown). In order to understand inconsistency in the sign of simulated horizontal moisture transport in the MME, we study their relative contribution to changes in vertical/horizontal moisture transport and MPWP precipitation changes.

Enhanced total water vapor transport (sum of horizontal and vertical moisture transport) is predominantly controlled by thermodynamics. This is inferred from 10 out of 14 models. Nevertheless, dynamic enhancement of total water vapor transport cannot be neglected as it dominates in 4 of the 14 models (Fig. 2c). Thermodynamic enhancement of total water transport is mainly due to increase in vertical water vapor transport, less due to elevated horizontal moisture transport. In contrast, dynamic enhancement of total water vapor transport is mainly related to horizontal moisture transport. Both thermodynamic and dynamic processes increase simulated horizontal moisture transport during the MPWP (Fig. 2c). Inconsistencies in horizontal moisture transport anomaly across the PlioMIP2 MPWP MME can be explained by thermodynamic and dynamical processes, caused by changes in specific humidity and changes in circulation, respectively, and

nonlinear processes, caused by changes in both (not shown), contributing to the net horizontal water transport (Fig. 2c).

Contrasting control of thermodynamic and dynamic processes on tropical and subtropical monsoon precipitation: data–model comparison

We quantify relative contribution of different physical processes to monsoon precipitation from the average water vapor budget in the region and identify those that dominate the MPWP EASM precipitation anomaly (Fig. 2). However, our analysis lacks spatial detail due to the applied area average. This caveat impedes comparison of models and records and limits physical interpretation of recorded precipitation anomalies. To enable reconciliation of model- and data-based anomalies, we therefore show in Fig. 3 the spatial distribution of thermodynamically and dynamically controlled enhancement of moisture transports.

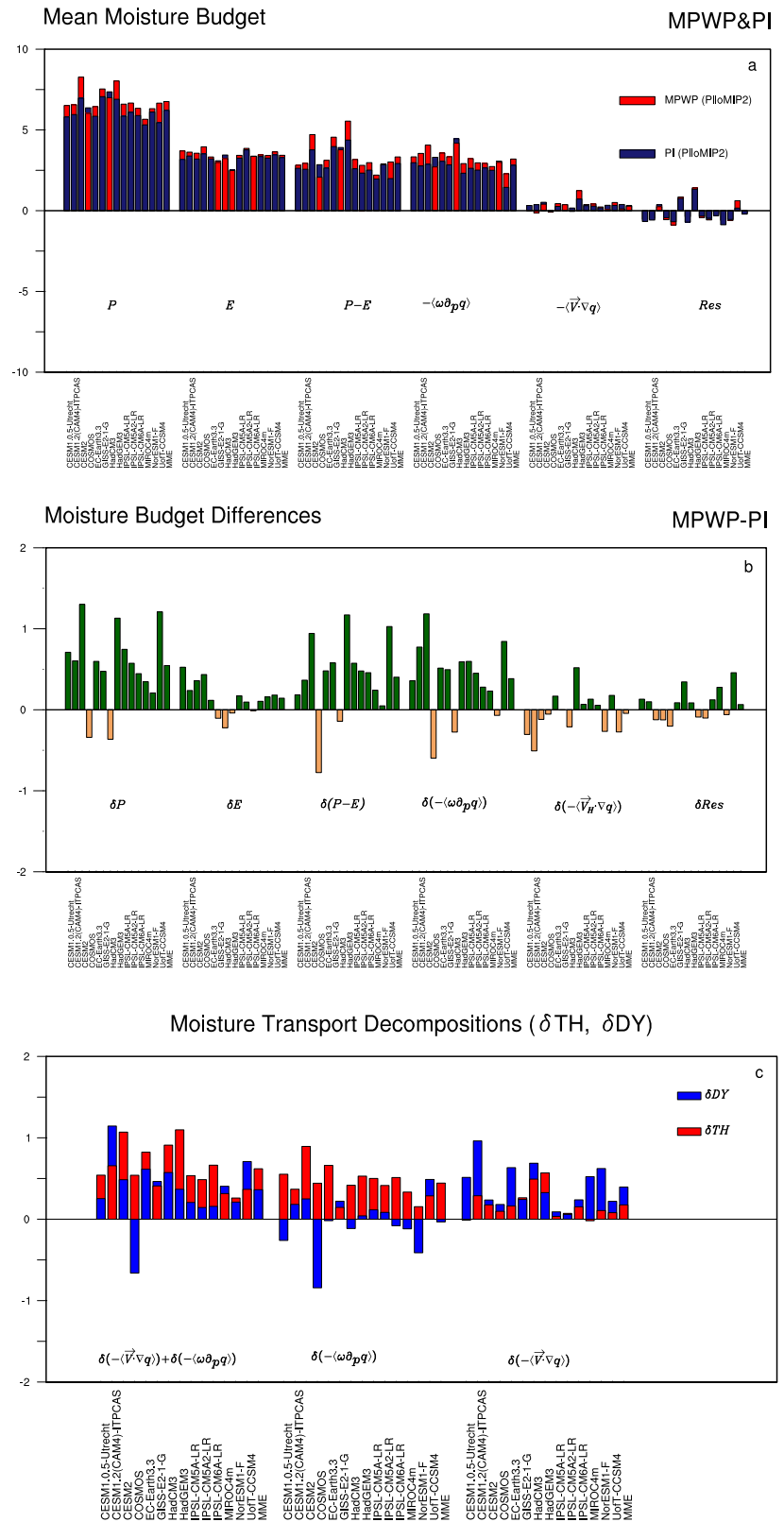
The thermally controlled enhancement of water vapor transport facilitates overall enhancement of EASM precipitation during the MPWP (compare Fig. 3a and Fig. 1d) mainly via thermodynamic control on increased vertical water vapor transport. In the tropics enhanced vertical water vapor transport contributes to an increase in EASM precipitation in reconstruction (1 of 25 records) and simulation (Fig. 3c). Although the thermodynamic component of horizontal water vapor transport largely increases area average EASM precipitation during the MPWP (Fig. 2c), its contribution is not spatially uniform (Fig. 3b). The pattern of enhanced horizontal moisture transport due to thermodynamic contribution, which in turn increases EASM precipitation during the MPWP, is opposed by a reduction in the southern part of northern China. Regional decrease in precipitation in 2 of the 25 pollen records may reflect this process (Fig. 3b).

There is regional diversity in the contribution of horizontal and vertical circulation changes to MPWP total water vapor transport anomalies. Dynamical processes significantly increase water vapor transport towards the subtropics, while water vapor transport to the remaining monsoon region is significantly reduced (Fig. 3d).

Enhanced subtropical water vapor transport mainly derives from enhanced horizontal circulation (Supplementary Fig. 2). Regional increase in precipitation in 12 of the 25 records (10 within the EASM domain and 2 outside the EASM domain) can be explained by the dynamically enhanced subtropical water vapor transport (Fig. 3e). In contrast, reduced water vapor transport to the remaining monsoon region is mainly due to reduced vertical transport linked to dynamically weakened vertical motion. This process explains the decrease in EASM precipitation in three records (Fig. 3f). In contrast, dynamics enhance the vertical moisture transport outside the EASM domain, explaining the increase of precipitation in six records in the region (Fig. 3f). Furthermore, reduced precipitation recorded at one location in the northwest margin of the EASM can be explained by weakened horizontal vapor transport due to weakened horizontal circulation (Fig. 3e).

In short, thermally controlled increase in horizontal and vertical moisture transports determines the overall enhancement of EASM precipitation during the MPWP. Enhanced tropical and subtropical EASM precipitation is in both records and simulations controlled by enhanced vertical moisture transport (thermodynamics) and by increased horizontal moisture transport (dynamics), respectively. This reflects two distinct sources of water vapor for enhanced regional monsoon precipitation (Fig. 4): one from the Bay of Bengal (tropical source) and the other from the western Pacific subtropical high (WPSH) (subtropical source). The latter contributes more to the increase in regional monsoon precipitation due to enhanced WPSH (Supplementary Movie 1). In addition to contrasting control of thermodynamic and dynamic processes on enhancement of tropical and subtropical monsoon precipitation, recorded and simulated reduction of tropical and subtropical monsoon precipitation is also controlled by the two different physical processes. Reduced thermodynamic contribution to horizontal water vapor transport explains decreases in subtropical EASM precipitation, whereas reductions in tropical EASM precipitation are dynamically controlled by the reduced vertical water vapor transport due to weakened vertical motion.

Fig. 2 | Moisture budget analysis calculated over the EASM monsoon domains (units: mm/day). **a** Mean JJA budget for MPWP and PI periods and **b** difference in the mean budget between the two periods; **c** thermodynamic and dynamic decomposition of moisture transport changes that contribute to MPWP EASM precipitation anomalies. The analysis is based on an average of simulated climate patterns over the monsoon domain.

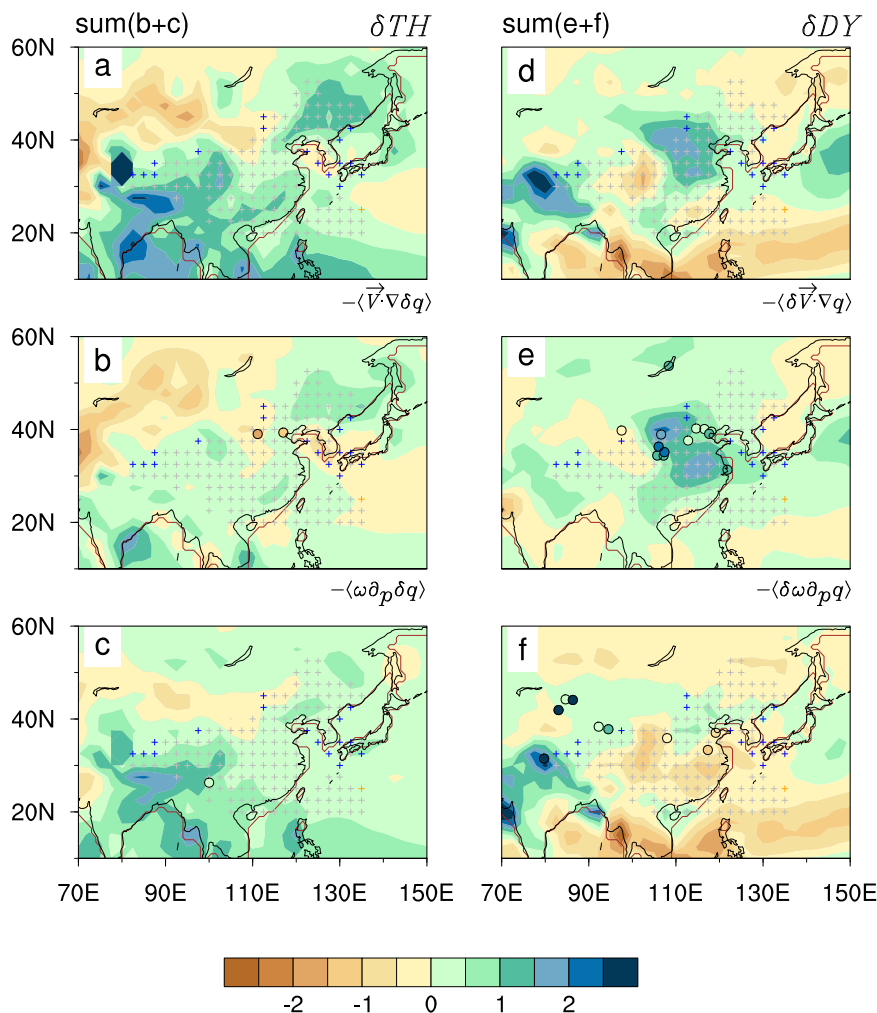


Paleoclimate perspectives constrain near-term future monsoon dynamics

The greenhouse gas single-factor experiments provided by PlioMIP2 and CMIP6 offer the opportunity to compare similarities and differences in the control of physical processes on monsoon for increased greenhouse gases in past and future. We show that elevated greenhouse gases increase monsoon

precipitation in two climatic contexts mainly through enhanced moisture transport regulated by thermodynamic effects that follow the Clausius-Clapeyron relationship (Fig. 5). That is, thermodynamics at stable elevated greenhouse forcing are shown to enhance both horizontal and vertical water vapor transport in two climate equilibrium states (Fig. 5, top and middle panels), while thermodynamics of a rapid increase in current greenhouse gas

Fig. 3 | Decomposed physical processes of precipitation used for site-by-site spatial matching with recorded precipitation. As Fig. 2c, but showing the spatial distribution of thermodynamic (a–c) and dynamic processes (d–f) in the MME which are used to decode the physical representations of pollen records by matching the pollen-based inference with thermodynamic and dynamic processes (colored circles).



concentrations increases monsoon precipitation mainly through enhanced vertical moisture transport (Fig. 5, bottom panel).

Similarly to variable mechanisms by which thermodynamics contribute to increased monsoon precipitation under stable or varying elevated greenhouse forcings, there are also contrasting effects of water vapor dynamics for equilibrium and transient climatic conditions. Dynamic effects increase monsoon precipitation in two equilibrium states while reducing it in transient climate (Fig. 5, left panel). Such distinct dynamical effects arise mainly from very different responses of horizontal circulation in the monsoon region in the two climatic contexts (Fig. 5, middle and right panels). In the two equilibrium states horizontal circulation responds to the increase in greenhouse gases with enhanced horizontal moisture transport. For ongoing rapid increase in greenhouse gases there is no contribution to horizontal moisture transport (Fig. 5, middle panel). The weakening effect of dynamical processes on water vapor transport for warming linked to current rapid increase in greenhouse gases is mainly due to suppressed water vapor transport caused by the reduced vertical circulation (Fig. 5, right panel). In contrast to relatively consistent changes in the area-averaged water budget (Fig. 5), response of monsoon precipitation (Supplementary Fig. 3) and thermodynamic and dynamical contributions to an increase in greenhouse gases is far from spatially uniform in the MME, both for equilibrium and transient climate states (Supplementary Fig. 4, Supplementary Fig. 10, Supplementary Fig. 15). We also find considerable variability among models even in the same climate state (Supplementary Fig. 5, Supplementary Fig. 6, Supplementary Fig. 7, Supplementary Fig. 8, Supplementary Fig. 9; Supplementary Fig. 11, Supplementary Fig. 12, Supplementary Fig. 13, Supplementary Fig. 14; Supplementary Fig. 16, Supplementary Fig. 17,

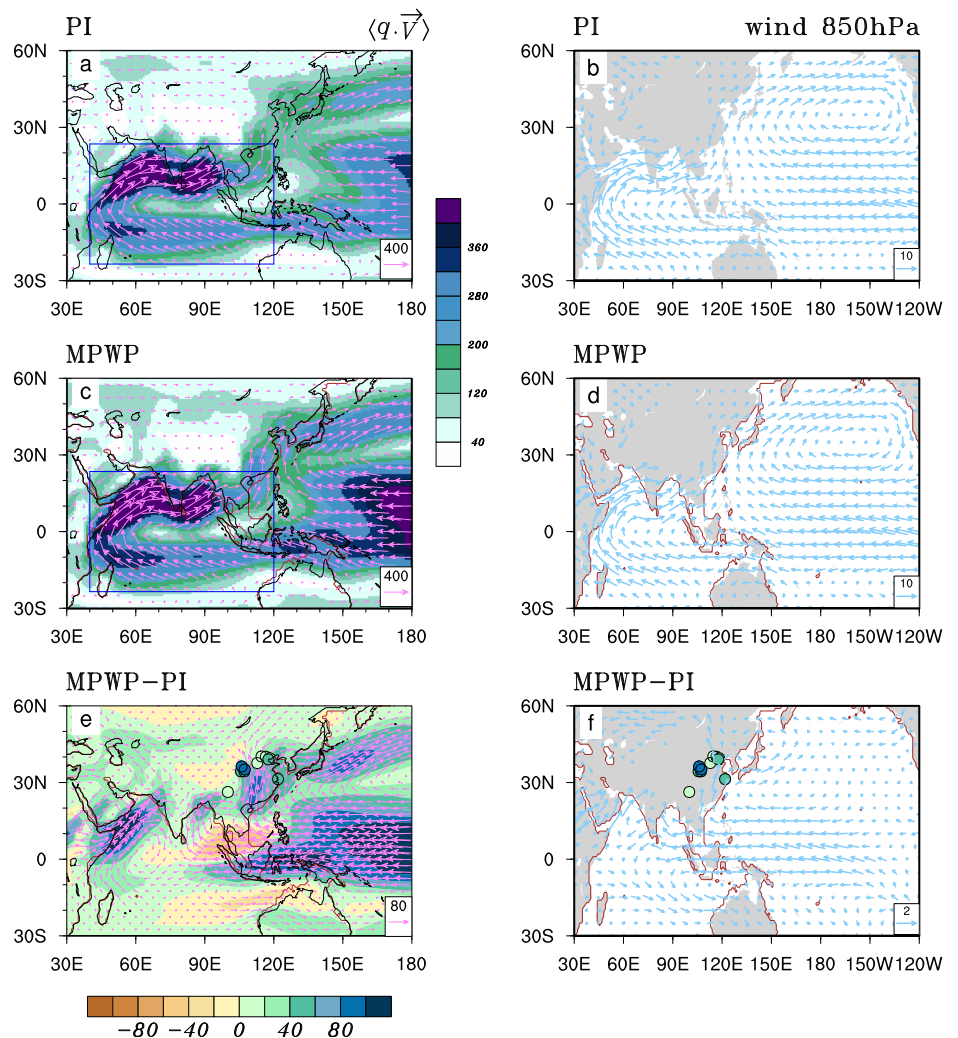
Supplementary Fig. 18, Supplementary Fig. 19, Supplementary Fig. 20). Uncertainty in past and future monsoon dynamics relate to each other.

Discussion

The EASM represents a hybrid tropical and subtropical summer monsoon system in East Asia. This study provides a quantitative model–data comparison of EASM precipitation anomalies MPWP vs. PI, allowing us to obtain information that may help understand and evaluate projections of EASM precipitation. By analyzing the moisture budget balance, we propose a new approach to reconcile the data–model discord of MPWP EASM precipitation anomalies. In addition to precipitation enhancement over the entire monsoon area that is controlled by thermodynamic processes, we highlight that the relative increase in tropical and subtropical MPWP EASM precipitation is controlled by thermodynamic and dynamical processes, respectively. This inference differs from overall enhancement of EASM precipitation under the impact of orbital forcing (mid-Holocene) under dynamic control³³. Consequently, we highlight that processes driving EASM behave differently depending on whether climate forcing is more associated to orbital parameters or to geography and substantial differences in greenhouse gas concentrations. We note that at centennial time-scales future climate is controlled more by the overall greenhouse gas concentration than by orbital or tectonic changes. The key findings of our study are summarized as follows:

1. We highlight data–model mismatch of MPWP EASM precipitation anomalies; spatially divergent precipitation changes inferred from records are opposed to a spatially nearly consistent increase in simulated EASM precipitation.

Fig. 4 | The sources of moisture that enhance tropical and subtropical EASM precipitation during the MPWP through thermodynamic and dynamic processes. Left panel: the vertically integrated water vapor transport throughout the troposphere is represented by the moisture fluxes ($\langle q \cdot \vec{V}_H \rangle$, units: $\text{kg m}^{-1} \text{s}^{-2}$) in JJA for PI (a) and MPWP periods (c) and the differences between MPWP and PI periods (e). Right panel: horizontal wind vector at 850 hPa (units: m s^{-1}) in JJA for PI (b), MPWP (d) and differences between MPWP and PI periods (f). The colored circles in (e, f) are 11 proxy records with precipitation increase within EASM domain. The strongest moisture pathway into the EASM domain, sustaining the mean state of EASM precipitation, is depicted by the blue rectangle in (a, c).



2. We propose the decomposition of monsoonal precipitation into contributions by relevant processes to reconcile inferences from data and model simulations. Overall, MPWP increases in EASM precipitation are controlled by thermodynamically enhanced vertical moisture transport. This is consistent with physical processes enhancing EASM precipitation under the impact of future anthropogenic warming²⁷ but differs from dynamical enhancement of EASM precipitation mainly via enhanced horizontal moisture transport at orbital time scales³³.
3. In addition to the overall thermal control, thermodynamic and dynamic processes tend to dominate with respect to tropical and subtropical MPWP EASM precipitation anomalies. The thermodynamic increase of vertical moisture transport towards the tropical EASM region enhances precipitation recorded and simulated there. Dynamical enhancement of precipitation on the other hand is evident in recorded and simulated subtropical EASM. In addition to enhancing tropical and subtropical EASM precipitation, both thermodynamic and dynamic processes control regional decrease in EASM precipitation. Reduced vertical water vapor transport under dynamic control may explain recorded decrease of subtropical EASM precipitation, while thermodynamic decrease in horizontal moisture transport provides an explanation of recorded reduction in another part of subtropical EASM precipitation.
4. Both thermodynamic and dynamical effects enhance regional tropical and subtropical EASM precipitation in records and simulations during the MPWP, reflecting the two different sources of water vapor that enhance monsoon precipitation. The thermodynamic enhancement of

- tropical EASM precipitation originates from enhanced water vapor transport in the tropical Indian Ocean and the dynamic increase in subtropical EASM precipitation due to enhanced water vapor transport by western Pacific subtropical high.
5. The dynamics of the EASM under elevated greenhouse gases in the past warm period exhibit similar traits to those anticipated under increasing greenhouse gases in future projection scenarios. In both cases, a thermally controlled increase in EASM precipitation is observed. This insight stands as a significant outcome from our investigation into monsoon dynamics during the past warm period.

In conclusion, through the decomposition of physical processes controlling EASM precipitation, we identified that (i) certain physical processes do align with the changes in recorded precipitation. (ii) Areas, where the sum of the decomposed physical processes does not align with the sign of the recorded precipitation, are indicative of biases in the simulated magnitude of the relative contribution of the decomposed physical processes to the total simulated precipitation response. These biases require improvement in the models. (iii) The proposed decomposition of the monsoon precipitation process in this study serves not only to reconcile the comparison between records and simulations in the East Asian monsoon region but also facilitates the comparison of precipitation records and simulations in tropical monsoon areas. Moreover, it extends its utility to the comparison of precipitation records and simulations outside the monsoon region.

The variations in orbital parameters during the Pliocene can influence monsoon precipitation^{34,35}. While the PlioMIP2 protocol did not consider

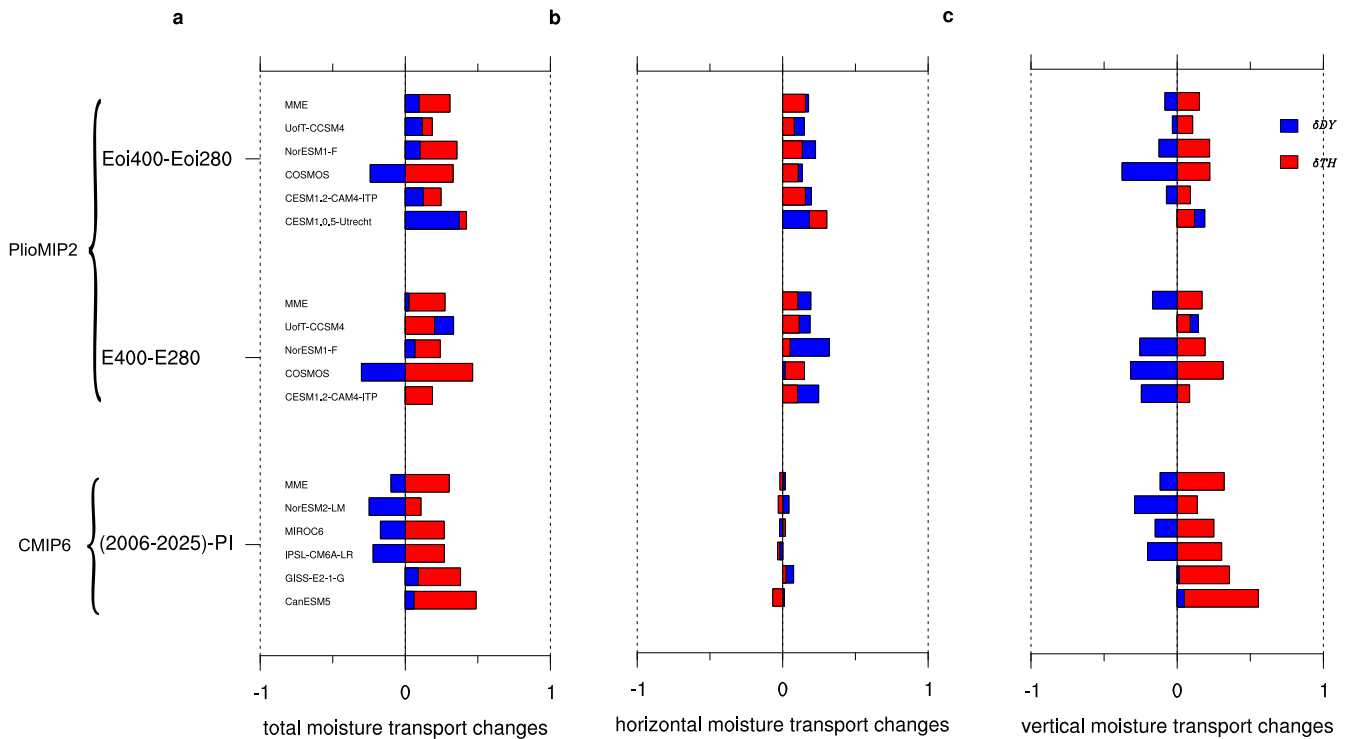


Fig. 5 | Comparison of the decomposed physical processes of monsoon precipitation: past warmth vs. future warming. As Fig. 2c, but separating thermodynamic and dynamical contributions to moisture transport (units: mm/day) in response to similar CO₂ increase in two climate contexts, including MPWP (top); PI

(middle); and current transient warming relative to the PI period (bottom). From left to right: thermodynamic and dynamical decompositions of changes in total moisture transport, changes in horizontal moisture transport, changes in vertical moisture transport.

changes in orbital parameters, this will be an optional experiment in the upcoming PlioMIP3³⁶. In addition, the inclusion of aerosol emissions during the Pliocene³⁷ and the growth of the Antarctic ice sheet from the Miocene to the Pliocene³⁸ in the models could provide potential opportunities to improve consistency between simulations and records. In addition, the number of model members used for ensemble average may also influence the spatial distribution of the Pliocene monsoon precipitation response (Fig. 1d and Supplementary Fig. 21).

Methods

Proxy records of East Asian during the MPWP

We compiled 25 published MPWP fossil pollen records across East Asia, ensuring that they exhibit clear and complete pollen spectra with a resolution higher than 60 ka. All records are based on paleomagnetic or other precise dating methods (e.g., Electron Spin Resonance - ESR) to provide reliable age data, with the paleomagnetic age dates calibrated according to the latest geomagnetic polarity time scale³⁹.

Precipitation is quantitatively derived using the Modern Analogue Technique⁴⁰ due to its advantages in large-scale reconstructions⁴¹. To address the lack of modern analogs^{42,43}, we utilize Plant Functional Type scores in the calculation of squared chord distance⁴⁴. More detailed descriptions can be found in the Supplementary Text 1 and Supplementary table 1.

PlioMIP2 core simulations

Precipitation differences in MPWP (Eoi400) with regard to pre-industrial (E280) as simulated in the PlioMIP2 are quantitatively compared with pollen-based reconstructed precipitation. This analysis is supported with climate dynamics analysis methods to extract the physical representation of precipitation in the records.

The PlioMIP2 protocol¹² required modeling groups to follow a common procedure towards the setup of MPWP simulations. PlioMIP2 simulations selected for our study (Supplementary Table 2) focus

on some of the key changes including: a) the atmospheric CO₂ concentration is set to 400 ppm; b) Greenland ice cover is reduced to 25% of the pre-industrial (PI) period³; c) terrestrial vegetation is derived from reconstruction by ref. 45; d) minor tectonic changes with regard to modern geography include the closure of the Bering Strait, Hudson Bay and Canadian Arctic Archipelago, as well as further reconfigurations of coastlines and ocean bathymetry as a result of strongly reduced West Antarctic Ice Sheet and changes at Kara Strait, Java Sea, Torres Strait, and South China Sea¹². However, not all groups implemented all of these tectonic changes¹³, and HadGEM3 did not implement any of them⁴⁶. Fourteen models who contributed MPWP simulations to PlioMIP2 were considered in this study (Supplementary table 2). Importantly, all PlioMIP2 models used in this study show robust performance in simulating the East Asian monsoon climate, as demonstrated in the works^{27,30,47–51}. The last 30 years of simulations served to analyze EASM and related climate patterns.

Nevertheless, state-of-the-art climate models exhibit biases in the simulation of regional precipitation, and although high-resolution models are recommended for improvement⁵², their universal added value is not guaranteed⁵³. Analysis of high-resolution MIP models⁵⁴ shows that even with high-resolution simulations attempting to address these issues, the prevalent dry biases persist in low-resolution simulations in core Asian monsoon regions. Increasing model resolution alone has limited effectiveness in improving total mean precipitation but can improve the model's ability to simulate extreme precipitation^{54,55}.

To reduce uncertainty in individual model simulations, a MME mean of PlioMIP2 models is employed for comparison with proxy data. This approach is considered superior, as the ensemble mean's skill can exceed that of individual models⁵².

Individual greenhouse gas (GHG) experiment following the PlioMIP2 and CMIP6 protocols

To isolate the effects of increased greenhouse gas concentrations (relative to PI) on monsoonal precipitation and its physical processes, we additionally

analyzed single-factor greenhouse gas experiments conducted in three different climate contexts in PlioMIP2 and Coupled Model Intercomparison Project Phase 6 (CMIP6) (Supplementary table 3). These include an experiment conducted at equilibrium with MPWP geography as PlioMIP2 core simulation Eoi400 but where CO₂ concentrations were reduced to the same level as in the PI (Eoi280); an experiment based on PI geography as E280, but where CO₂ concentrations were increased to the same level as in the MPWP core simulation (E400); and experiments with similar increases in CO₂ concentrations (compared to the PI) taken from ongoing transient climate (2006–2025).

Diagnostic methodology

The moisture budget equation is suitable to identify the mechanism causing EASM precipitation anomalies, MPWP with respect to PI, because it incorporates the physical processes that affect precipitation^{33,56,57}. The time-mean air column integral of this equation throughout the troposphere can be written as:

$$P = E - \langle \omega \partial_p q \rangle - \langle \mathbf{V}_H \cdot \nabla q \rangle + Res \tag{1}$$

where P is the precipitation, E is the evaporation, ω is the vertical velocity, q is the atmospheric specific humidity, \mathbf{V}_H is the horizontal wind, and Res is the residual term that includes transient eddy effects and deformation of the surface moisture transport by the surface pressure gradient^{33,58}. The bracket notation refers to the vertical integral of the atmospheric column across the troposphere. $\langle \cdot \rangle = \frac{1}{g\rho_w} \int_0^{P_s} \cdot dp$, where P_s is the surface pressure, ρ_w is the density of water, and g is the gravitational acceleration. The first bracket on the right-hand side of Eq. (1) refers to vertical moisture advection whereas the second term describes horizontal transport of water vapor.

The relative importance of each physical process in Eq. (1) for differences in precipitation between two climates (e.g., MPWP relative to the PI), i.e., δP , can be derived from the difference in the water vapor budget balance between the two periods (Eqs. 2 and 3).

$$\delta P = \delta E - \delta \langle \omega \partial_p q \rangle - \delta \langle \mathbf{V}_H \cdot \nabla q \rangle + \delta Res \tag{2}$$

$$\begin{aligned} \approx & \delta E - \langle \delta \omega \partial_p q \rangle - \langle \omega \partial_p \delta q \rangle - \langle \delta \omega \partial_p \delta q \rangle - \langle \delta \mathbf{V}_H \cdot \nabla q \rangle \\ & - \langle \mathbf{V}_H \cdot \nabla \delta q \rangle - \langle \delta \mathbf{V}_H \cdot \nabla \delta q \rangle + \delta Res \end{aligned} \tag{3}$$

Thermodynamic and dynamic decomposition of changes in second and third terms on the right hand side of Eq. (2) are conducted to further distinguish between relative contributions of changes in water vapor transport by thermodynamic and dynamic processes. For example, the thermodynamic contribution results from changes in specific humidity at fixed atmospheric circulation (due to increased water holding capacity of warmer air according to the Clausius-Clapeyron equation) whereas the dynamic contribution is caused by atmospheric circulation changes at constant specific humidity. The contribution of both changes in atmospheric circulation and changes in specific humidity to changes in water vapor transport is called the nonlinear term and is usually neglected because it is smaller compared to the other terms.

Thermodynamic (TH), dynamic (DY) and nonlinear (NL) components of changes in vertical moisture transport can be written as follows:

$$\delta TH = - \langle \omega \partial_p \delta q \rangle = - \frac{1}{g\rho_w} \int_0^{P_s} \omega \partial_p \delta q dp \tag{4}$$

$$\delta DY = - \langle \delta \omega \partial_p q \rangle = - \frac{1}{g\rho_w} \int_0^{P_s} \delta \omega \partial_p q dp \tag{5}$$

$$\delta NL = - \langle \delta \omega \partial_p \delta q \rangle = - \frac{1}{g\rho_w} \int_0^{P_s} \delta \omega \partial_p \delta q dp \tag{6}$$

Here we extend the work of Chou and Lan⁵⁷ and decompose horizontal moisture transport in addition to vertical moisture transport^{33,59}. Changes in horizontal moisture transport were further decomposed into thermodynamic (δTH) and dynamic contributions (δDY):

$$\delta TH = - \langle \mathbf{V}_H \cdot \nabla \delta q \rangle = - \frac{1}{g\rho_w} \int_0^{P_s} \mathbf{V}_H \cdot \nabla \delta q dp \tag{7}$$

$$\delta DY = - \langle \delta \mathbf{V}_H \cdot \nabla q \rangle = - \frac{1}{g\rho_w} \int_0^{P_s} \delta \mathbf{V}_H \cdot \nabla q dp \tag{8}$$

$$\delta NL = - \langle \delta \mathbf{V}_H \cdot \nabla \delta q \rangle = - \frac{1}{g\rho_w} \int_0^{P_s} \delta \mathbf{V}_H \cdot \nabla \delta q dp \tag{9}$$

Data availability

Proxy data is available online (https://figshare.com/articles/dataset/Pollen-based_precipitation_reconstruction_for_the_mid-Piacenzian_Warm_Period/23732988); Access to the PlioMIP2 climate model data is available online (https://figshare.com/articles/dataset/PlioMIP2_data_available_for_EASM_dynamics/23849298); Access to the CMIP6 individual GHG experiment is available online (<https://esgf-node.llnl.gov/projects/cmip6/>).

Code availability

The codes for creating the figures and analyses were written in NCAR Command Language Version 6.5 and are available on request from the corresponding author.

Received: 14 November 2023; Accepted: 14 May 2024;

Published online: 05 June 2024

References

1. Robinson, M. M., Dowsett, H. J. & Chandler, M. A. Pliocene role in assessing future climate impacts. *Trans. Am. Geophys. Union* **89**, 501–502 (2008).
2. Harrison, S. P. et al. Evaluation of CMIP5 palaeo-simulations to improve climate projections. *Nat. Clim. Change* **5**, 735–743 (2015).
3. Tierney, J. E. et al. Past climates inform our future. *Science* **370**, eaay3701 (2020).
4. Burke, K. D. et al. Pliocene and Eocene provide best analogs for near-future climates. *Proc. Natl Acad. Sci. USA* **115**, 13288–13293 (2018).
5. Dowsett, H. J. et al. Joint investigations of the Middle Pliocene climate I: PRISM paleoenvironmental reconstructions. *Glob. Planet. Change* **9**, 169–195 (1994).
6. Dowsett, H. J., Barron, J. A. & Poore, R. Z. Middle Pliocene sea surface temperatures: a global reconstruction. *Mar. Micropaleontol.* **27**, 13–25 (1996).
7. Dowsett, H. J. et al. Middle pliocene palaeoenvironmental reconstruction: PRISM 2, *US Geol. Surv.*, Open File Report 99–535 (1999).
8. Dowsett, H. J. et al. The PRISM3D paleoenvironmental reconstruction. *Stratigraphy* **7**, 123–139 (2010).
9. Dowsett, H. J. et al. The PRISM4 (mid-Piacenzian) paleoenvironmental reconstruction. *Clim. Past* **12**, 1519–1538 (2016).
10. Haywood, A. M. et al. Large-scale features of Pliocene climate: results from the Pliocene Model Intercomparison Project. *Clim. Past* **9**, 191–209 (2013).
11. Salzmann, U. et al. Challenges in quantifying Pliocene terrestrial warming revealed by data–model discord. *Nat. Clim. Change* **3**, 969–974 (2013).
12. Haywood, A. M. et al. The Pliocene Model Intercomparison Project (PlioMIP) Phase 2: scientific objectives and experimental design. *Clim. Past.* **12**, 663–675 (2016).

13. Haywood, A. M. et al. The Pliocene Model Intercomparison Project Phase 2: large-scale climate features and climate sensitivity. *Clim. Past* **16**, 2095–2123 (2020).
14. Haywood, A. M., Dowsett, H. J. & Tindall, J. C. PlioMIP1 and PlioMIP2 participants. PlioMIP: the Pliocene Model Intercomparison Project. *Glob. Chang. Mag.* **29**, 92–93 (2021).
15. Zhu, Q., He, J. & Wang, P. A study of circulation differences between East-Asian and Indian summer monsoons with their interaction. *Adv. Atmos. Sci.* **3**, 466–477 (1986).
16. Liu, Z. et al. Chinese cave records and the East Asia Summer Monsoon. *Quat. Sci. Rev.* **83**, 115–128 (2014).
17. Tan, M. Is the East Asian summer paleomonsoon a tropical or subtropical monsoon?—And discussion on “Why climatologists don’t draw the EASM arrow?”. *Quater. Inter.* **36**, 1518–1519 (2016).
18. IPCC. Annex V: Monsoons [Cherchi, A., A. Turner (eds.)]. In *Climate Change 2021: The Physical Science Basis*. Contribution of Working Group I to the Sixth Assessment Report of the Intergovernmental Panel on Climate Change [Masson-Delmotte, V., et al. (eds.)]. Cambridge University Press, Cambridge, United Kingdom and New York, NY, USA, pp. 2193–2204 (2021).
19. Liu, X. et al. Where were the monsoon regions and arid zones in Asia prior to the Tibetan Plateau uplift. *Natl Sci. Rev.* **2**, 403–416 (2015).
20. Yan, H. et al. Dynamics of the intertropical convergence zone over the western Pacific during the Little Ice Age. *Nat. Geosci.* **8**, 315–320 (2015).
21. Wang, B., Liu, J., Kim, H., Webster, P. J. & Yim, S. Y. Recent change of the global monsoon precipitation (1979–2008). *Clim. Dyn.* **39**, 1123–1135 (2012).
22. Kitoh, A. The Asian monsoon and its future change in climate models: a review. *J. Meteorol. Soc. Jpn.* **95**, 7–33 (2017).
23. Wang, B., Yim, S. Y., Lee, J., Liu, J. & Ha, K. Future change of Asian-Australian monsoon under RCP 4.5 anthropogenic warming scenario. *Clim. Dyn.* **42**, 83–100 (2013).
24. Jin, C., Wang, B. & Liu, J. Future changes and controlling factors of the eight regional monsoons projected by CMIP6 models. *J. Clim.* **33**, 9307–9326 (2020).
25. IPCC. Water Cycle Changes. In *Climate Change 2021—The Physical Science Basis: Working Group I Contribution to the Sixth Assessment Report of the Intergovernmental Panel on Climate Change* (pp. 1055–1210). (IPCC, Cambridge University Press, 2023).
26. Li, Z., Sun, Y., Li, T., Ding, Y. & Hu, T. Future changes in East Asian summer monsoon circulation and precipitation under 1.5 to 5 °C of warming. *Earth’s Future* **7**, 1391–1406 (2019).
27. Sun, Y. et al. Quantifying East Asian Summer Monsoon Dynamics in the ECP4.5 Scenario With Reference to the Mid-Piacenzian Warm Period. *Geophys. Res. Lett.* **45**, 12,523–12,533 (2018).
28. Feng, R., Otto-Bliesner, B. L., Brady, E. C. & Rosenbloom, N. A. Increased climate response and earth system sensitivity from CCSM4 to CESM2 in mid-pliocene simulations. *J. Adv. Model. Earth Syst.* **12** (2020).
29. Feng, R. et al. Past terrestrial hydroclimate sensitivity controlled by Earth system feedbacks. *Nat. Commun.* **13** (2022).
30. Zhang, R. et al. Mid-Pliocene East Asian monsoon climate simulated in the PlioMIP. *Climate* **9**, 2085–2099 (2013).
31. Yan, Q., Wei, T. & Zhang, Z. Reexamination of the late pliocene climate over china using a 25-km resolution general circulation model. *J. Clim.* **32**, 897–916 (2019).
32. Han, Z. et al. Evaluating the large-scale hydrological cycle response within the Pliocene Model Intercomparison Project Phase 2 (PlioMIP2) ensemble. *Clim Past* **17**, 2537–2558 (2021).
33. Sun, Y. et al. Revisiting the physical mechanisms of East Asian summer monsoon precipitation changes during the mid-Holocene: a data–model comparison. *Clim. Dyn.* **60**, 1009–1022 (2023).
34. Yan, Q., Zhang, Z. & Zhang, R. Investigating sensitivity of East Asian monsoon to orbital forcing during the Late Pliocene warm period. *J. Geophys. Res. Atmos.* **123**, 7161–7178 (2018).
35. Zhang, R., Jiang, D. & Zhang, Z. Causes of mid-Pliocene strengthened summer and weakened winter monsoons over East Asia. *Adv. Atmos. Sci.* **32**, 1016–1026 (2015).
36. Haywood, A. M. et al. Pliocene Model Intercomparison Project Phase 3 (PlioMIP3) – Science Plan and Experimental Design. *Glob. Planet. Change*, <https://doi.org/10.1016/j.gloplacha.2023.104316> (2024).
37. Shi, Z. et al. Simulated variations of eolian dust from inner Asian deserts at the mid-Pliocene, last glacial maximum, and present day: contributions from the regional tectonic uplift and global climate change. *Clim. Dyn.* **37**, 2289–2301 (2011).
38. Ao, H. et al. Late Miocene–Pliocene Asian monsoon intensification linked to Antarctic ice-sheet growth. *Earth Planet. Sci. Lett.* **444**, 75–87 (2016).
39. Ogg, J. G. Geomagnetic polarity time scale. *Geol. Time Scale* **2020**, 159–192 (2020).
40. Overpeck, J. T., Webb, T. & Prentice, I. C. Quantitative interpretation of fossil pollen spectra: dissimilarity coefficients and the method of modern analogs. *Quat. Res.* **23**, 87–108 (1985).
41. Chevalier, M. et al. Pollen-based climate reconstruction techniques for late Quaternary studies. *Earth. Sci. Rev.* **210**, 1–33 (2020).
42. Davis, B., Brewer, S. C., Stevenson, A. C. & Guiot, J. The temperature of Europe during the Holocene reconstructed from pollen data. *Quat. Sci. Rev.* **22**, 1701–1716 (2003).
43. Peyron, O. et al. Climatic reconstruction in Europe for 18,000 YR B.P. *Pollen Data. Quat. res.* **49**, 183–196 (1998).
44. Prentice, I. C. et al. Special Paper: A global biome model based on plant physiology and dominance, soil properties and climate. *J. Biogeogr.* **19**, 117–134 (1992).
45. Salzmann, U., Haywood, A. M., Lunt, D. J., Valdes, P. J. & Hill, D. J. A new global biome reconstruction and data-model comparison for the Middle Pliocene. *Glob. Ecol. Biogeogr.* **17**, 432–447 (2008).
46. Williams, C. J. et al. Simulation of the mid-Pliocene Warm Period using HadGEM3: experimental design and results from model–model and model–data comparison. *Clim. Past* **17**, 2139–2163 (2021).
47. Jiang, D., Wang, H. & Lang, X. Evaluation of East Asian climatology as simulated by seven coupled models. *Adv. Atmos. Sci.* **22**, 479–495 (2005).
48. Jiang, D., Tian, Z. & Lang, X. Mid-Holocene net precipitation changes over China: model–data comparison. *Quat. Sci. Rev.* **82**, 104–120 (2013).
49. Jiang, D. B., Hu, D., Tian, Z. P. & Lang, X. M. Differences between CMIP6 and CMIP5 models in simulating climate over China and the East Asian monsoon. *Adv. Atmos. Sci.* **37**, 1102–1118 (2020).
50. Li, J., Wang, B. & Yang, Y. Diagnostic metrics for evaluating model simulations of the east Asian Monsoon. *J. Clim.* **33**, 1777–1801 (2020).
51. Zhang, Z. et al. Impact of mountains in southern China on the eocene climates of East Asia. *J. Geophys. Res. Atmos.* **127**, e2022JD036510 (2022).
52. Flato, G. et al. Evaluation of climate models. In: *Climate Change 2013: The Physical Science Basis. Contribution of Working Group I to the Fifth Assessment Report of the Intergovernmental Panel on Climate Change*. Cambridge University Press, Cambridge, United Kingdom and New York, NY, USA: pp 741–866 (2013).
53. Mishra, A. K., Dubey, A. K. & Dinesh, A. S. Diagnosing whether the increasing horizontal resolution of regional climate model inevitably capable of adding value: investigation for Indian summer monsoon. *Clim. Dyn.* **60**, 1925–1945 (2023).
54. You, Y. & Ting, M. Improved performance of high-resolution climate models in simulating Asian monsoon rainfall extremes. *Geophys. Res. Lett.* **50**, e2022GL100827 (2023).
55. Li, F. et al. Impact of horizontal resolution on simulation of precipitation extremes in an aqua-planet version of Community Atmospheric Model (CAM3). *Tellus A Dyn. Meteorol. Oceanogr.* **63**, 884–892 (2011).

56. Seager, R., Naik, N. & Vecchi, G. A. Thermodynamic and dynamic mechanisms for large-scale changes in the hydrological cycle in response to global warming. *J. Clim.* **23**, 4651–4668 (2010).
57. Chou, C. & Lan, C.-W. Changes in the annual range of precipitation under global warming. *J. Clim.* **25**, 222–235 (2012).
58. D'Agostino, R. & Lionello, P. The atmospheric moisture budget in the Mediterranean: mechanisms for seasonal changes in the Last Glacial Maximum and future warming scenario. *Quat. Sci. Rev.* **241**, 106392 (2020).
59. Sun, Y. et al. The contrasting effects of thermodynamic and dynamic processes on East Asian summer monsoon precipitation during the Last Glacial Maximum: a data-model comparison. *Clim. Dyn.* **56**, 1303–1316 (2021).
- C.W. for HadGEM3; A.A. and W.C. for MIROC4m; B.O. and R. F. for CESM2; G.L. and C.S. for COSMOS; G.R., C.C., and N.T. for IPSL-CM6A-LR, IPSL-CM5A-LR, and IPSL-CM5A2-LR; M. B. for CESM 1.0.5-Utrecht; Q.L. for EC-Earth3.3; W.P. and D.C. for UoF-CCSM4; Y.S. for CESM1.2(CAM4)-ITPCAS; Z.Z. for NorESM-F. H.D. directed the PRISM4 boundary conditions for PlioMIP2 and the 3 Ma vegetation reconstructed by U.S. All authors contributed to the final manuscript.

Competing interests

The authors declare no competing interests.

Additional information

Supplementary information The online version contains supplementary material available at <https://doi.org/10.1038/s41612-024-00668-4>.

Correspondence and requests for materials should be addressed to Yong Sun.

Reprints and permissions information is available at <http://www.nature.com/reprints>

Publisher's note Springer Nature remains neutral with regard to jurisdictional claims in published maps and institutional affiliations.

Open Access This article is licensed under a Creative Commons Attribution 4.0 International License, which permits use, sharing, adaptation, distribution and reproduction in any medium or format, as long as you give appropriate credit to the original author(s) and the source, provide a link to the Creative Commons licence, and indicate if changes were made. The images or other third party material in this article are included in the article's Creative Commons licence, unless indicated otherwise in a credit line to the material. If material is not included in the article's Creative Commons licence and your intended use is not permitted by statutory regulation or exceeds the permitted use, you will need to obtain permission directly from the copyright holder. To view a copy of this licence, visit <http://creativecommons.org/licenses/by/4.0/>.

© The Author(s) 2024

Acknowledgements

We acknowledge the World Climate Research Program's Working Group on Coupled Modelling for CMIP6 and thank climate modeling groups (listed in Fig. 2 and Fig. 5 of this paper) for producing and making available their model output. This study was funded by the Second Tibetan Plateau Scientific Expedition and Research Program (2019QZKK0708), the national key research and development program (No. 2022YFF0801504), the National Natural Science Foundation of China (42105048), the Basic Research Fund of Chinese Academy of Meteorological Sciences (2021Y019), Youth Innovation Team of China Meteorological Administration "Climate change and its impact in the Tibetan Plateau" (NO.CMA2023QN16). This work was supported by the National Key Scientific and Technological Infrastructure project "Earth System Numerical Simulation Facility" (EarthLab). G. L. and C. S. acknowledge institutional funding via the Helmholtz research program "Changing Earth - Sustaining our Future". C.S. acknowledges funding from the Helmholtz Climate Initiative REKLIM. R. F. acknowledges funding from National Science Foundation project number NSF-2103055.

Author contributions

Y.S., L.D., and H.W. conceived the study; Y.S. performed the dynamic analysis and wrote the draft manuscript; H. W., L.C., and W.Z. prepared the reconstructions of precipitation; C.S. edited the entire manuscript and contributed to the design of the study with regard to linking past and future monsoon dynamics (section 3.3). Y.Z., B.S., X.Y., B.L. assisted with the presentation. The following modeling groups contribute MPWP simulations following the PlioMIP2 protocol: A.H., S.H., A.D., J.T. for HadCM3; D.L. and

¹State Key Laboratory of Tibetan Plateau Earth System, Environment and Resources (TPESER), Institute of Tibetan Plateau Research, Chinese Academy of Sciences, Beijing 100101, China. ²Laboratoire des Sciences du Climat et de l'Environnement, LSCE/IPSL, CEA-CNRS-UVSQ, Université Paris-Saclay, Gif-sur-Yvette, France. ³Key Laboratory of Cenozoic Geology and Environment, Institute of Geology and Geophysics, Chinese Academy of Sciences, Beijing 100029, China. ⁴College of Earth and Planetary Sciences, University of Chinese Academy of Sciences, Beijing, China. ⁵Alfred-Wegener-Institut - Helmholtz-Zentrum für Polar und Meeresforschung, Bremerhaven, Germany. ⁶State Key Laboratory of Severe Weather, and Institute of Tibetan Plateau Meteorology, Chinese Academy of Meteorological Sciences, Beijing 100081, China. ⁷Institute of Atmospheric Physics, Chinese Academy of Sciences, Beijing 100029, China. ⁸School of Earth Sciences and Resources, China University of Geosciences (Beijing), Beijing 100083, China. ⁹Department of Atmospheric Science, School of Environmental Studies, China University of Geosciences, Wuhan 430074, China. ¹⁰School of Earth and Environment, University of Leeds, Woodhouse Lane, Leeds LS2 9JT, UK. ¹¹Atmosphere and Ocean Research Institute, University of Tokyo, Kashiwa, Japan. ¹²Climate and Global Dynamics Laboratory, National Center for Atmospheric Research, (NCAR), Boulder, CO 80305, USA. ¹³School of Geographical Sciences, University of Bristol, Bristol, UK. ¹⁴Department of Physics, University of Toronto, Toronto, ON M5S 1A7, Canada. ¹⁵Institut für Umweltphysik, Universität Bremen, Bremen, Germany. ¹⁶U.S. Geological Survey, 926 A National Center, Reston, VA 20192, USA. ¹⁷Institute for Marine and Atmospheric research Utrecht (IMAU), Department of Physics, Utrecht University, Utrecht 3584 CS, the Netherlands. ¹⁸Department of Physical Geography, Stockholm University, Stockholm 10691, Sweden. ¹⁹Department of Geosciences, College of Liberal Arts and Sciences, University of Connecticut, Storrs, CT 06033, USA. ²⁰Department of Geography and Environmental Sciences, Northumbria University, Newcastle upon Tyne NE1 8ST, UK. ²¹NORCE Norwegian Research Centre, Bjerknes Centre for Climate Research, Bergen, Norway. ✉ e-mail: yongsun@itpcas.ac.cn